Original scientific paper

TRIPLE-BAND STUB LOADED PATCH ANTENNA WITH HIGH GAIN FOR 5G SUB-6 GHZ, WLAN AND WIMAX APPLICATIONS USING DGS

Lalit Kumar, Vandana Nath, BVR Reddy

University School of Information, Communication and Technology,
Guru Gobind Singh Indraprastha University, New Delhi, India

Abstract. *Microstrip antennas have become ubiquitous in today's wireless communication world due to their low profile, low cost, and simplicity in fabricating on circuit boards. However, poor performance characteristics, such as limited bandwidth, low power handling capabilities, and low gain, limit their applicability in various instances. Path loss will be substantial in 5th generation (5G) wireless communication due to the utilization of high-frequency bands. A high-gain antenna with a small size is necessary to address this issue. A compact tri-band, slotted monopole antenna with high and consistent gain employing a defected ground plane structure (DGS) has been investigated and implemented in this study. This proposed antenna uses three inverted L-shaped stubs connected to the radiating element to cover the desired bands while keeping the antenna size small. The designed antenna has two key characteristics: (i) wide bandwidth and (ii) reasonable gain. The antenna covers 2.45 and 5.6 GHz WLAN, 2.4 GHz Wi-Fi, 2.5 and 5.2 GHz WiMAX and 3.7 GHz Sub-6 GHz of 5G for mobile communication. The overall substrate size of the antenna is $30 \times 17 \times 1.6$ mm³and the electrical dimensions are $0.49 \lambda_L \times 0.28 \lambda_L \times 0.026 \lambda_L$, where λ_L is the free space wavelength at 2.45 GHz. The measured reflection coefficient ($S_{11} < -10dB$) covers 2.4 - 2.52 GHz (bandwidth 112 MHz) and 3.4 - 4.1 GHz (bandwidth 700 MHz) and 5.2 - 6.6 GHz (bandwidth 1359 MHz) with a fractional bandwidth of 5.1 % at lower frequency band, 18.6 % at mid frequency band and 23.7 % at high frequency band. A prototype antenna has also been developed using an inexpensive, low-profile 1.6 mm thick FR-4 ($\varepsilon_r = 4.4$) substrate. The measured peak gains achieved are 1.35 dB at 2.45 GHz, 2.55 dB at 2.65 GHz and 3.8 dB at 5.5 GHz. The simulated results have been validated against actual experimental measurements, and the outcomes are consistent and match with certainty. The proposed antenna design is very compact and easy to fabricate due to the absence of vias.*

Key words: *5G Sub-6 GHz, slotted patch antenna, monopole, multiband, wide bandwidth*

1. Introduction

The advancement of mobile technology and the continuously reducing size of mobile devices has necessitated antenna designers to design antennas that can operate across multiple frequency bands while still compact and having adequate gain and efficiency. Antennas with multiple frequency bands and small sizes can be employed in mobile devices. Furthermore, high-gain antennas are highly beneficial for satellite communication applications. Broadband antennas have also grown in popularity in recent years. However, while the microstrip patch antenna offers the advantages of low cost and tiny size, it has the limitations of poor gain and narrow bandwidth. Other requirements include a low profile, simple design, ease of fabrication and low cost. These make planar microstrip patch antennas a better and more popular choice [1]. In addition, it is challenging to cover multiple bands while keeping the antenna size minimal with adequate bandwidth and gain [2].

The Sub-6 GHz frequency offers high-speed data transfer over long distances owing to its low latency and high traffic density. These features of the Sub-6 GHz frequency band are suitable for access points (AP) and base stations (BS) communication for machine-to-machine(M2M), Internet of Things (IoT) and device-to-device (D2D) technologies, along with existing WiMAX, WLAN, and LTE bands [3]. A practical solution for such a system design is a multiband antenna with a frequency band selection capability. Several printed monopole antennas with different geometries are demonstrated with a reduced size while increasing bandwidth to meet WLAN, WiMAX, and 5G Sub-6 GHz technology standards [3]. Therefore, modifying an antenna's geometry to occupy a small volume is necessary to reduce its overall size. It is worth mentioning that stub matching and slotting techniques are widely used to maintain the compactness of the antenna. The stubs increase the current path length to get a fundamental resonating mode [4-8]. For improving impedance matching in multiband operations while reducing antenna volume, slots of different types and geometries are implemented [9-13]. In the present era of antenna design, one of the most important considerations is how to maximise the bandwidth of compact antennas. Therefore, many researchers have suggested diverse techniques to develop a small antenna with broadband characteristics with multiband operations. Some proposed methods include a thick substrate, shorting pins, active and passive devices, stacked patches, various feeding mechanisms and an impedance-matching network. Defected Ground Structure (DGS) is one such type of bandwidth enhancement technique where some defects are introduced, or slots are carved in the ground plane to suppress the cross-polarisation radiation, reduce the antenna size and achieve the desired performance [14-18].

M. Karthieyen et al. [7] proposed a tri-band antenna using T-shaped strips and rectangular slot defects at the ground side. The proposed antenna operates at three frequency bands, viz. 2.47-2.77 GHz, 3.3-3.7 GHz and 5.10-6.62 GHz. The FR-4 substrate dimensions are $33 \times 17 \times 1.6$ mm^3. The average gain ranges from 2 to 3.9 dB, but the efficiency ranges from 60% to 80%, covering WLAN and WiMAX bands only. Using an arc-shaped DGS, a planar monopole antenna for triple-band operation is proposed in [11] for wireless LAN and WiMAX bands. The proposed antenna combines monopole rings and a defective ground plane. Monopoles are made up of a rectangular ring and a rectangular patch connected by a straight metal strip that may create lower- and middle-frequency bands and omnidirectional radiation patterns. The substrate is FR-4 with 1.6 mm thickness, but a relatively larger antenna size is 36×39 mm^2. Antenna resonates at 2.45 GHz, 3.55 GHz and 5.5 GHz and 1.22 dB, 2.15 dB and 4.06 dB gain and 88%, 99% and 94% efficiencies in the respective

bands. A small slotted monopole antenna is presented by H. Ahmed et al. [19] for wireless LAN and WiMAX frequency bands. Resonance in three bands has been achieved by etching a rectangle patch with bevel, Pi, and inverted L-shaped slots. The antenna is 27.5×20 mm^2 in size and operates in three bands: 2.37 - 2.52 GHz, 3.35 - 3.90 GHz, and 4.97 - 7.85 GHz. The antenna radiation pattern is almost omnidirectional, having 90 % efficiency and 4 dBi gain across the three WLAN and WiMAX frequency ranges. In [20], a multiband monopole antenna is presented using a rectangular patch etched with two crossed C- shaped slots and two E - shaped slots in a curtailed ground plane. The total dimension of the antenna is $29 \times 36 \times 0.8$ mm^3, and the antenna casts on an FR-4 substrate. The antenna achieves a maximum gain of 2.5 dBi and maximum efficiency of 98 % at a higher frequency band, and it covers both the wireless LAN and WiMAX frequency bands. But antenna has a comparatively lower gain and larger size.

Defected ground structure (DGS) has been utilised in microstrip antennas to increase the bandwidth and gain and suppress higher mode harmonics, mutual coupling between neighbouring elements, and cross-polarisation to improve the radiation properties of microstrip antennas. For WLAN / WiMAX applications, A. Ibrahim et al. [21] have developed an antenna using DGS for tri-band operations. The antenna has relatively lower bandwidths of 197 MHz, 118 MHz, and 90 MHz and resonates at three frequencies: 2.4 GHz, 3.5 GHz, and 5.8 GHz. The substrate is FR-4, with a dielectric constant of 4.3 and larger dimensions of $34 \times 30 \times 1.6$ mm^3. In [22], a triple-band antenna structure using a defective ground plane is suggested for use in WLAN, WiMAX, and Wi-Fi applications. The proposed antenna achieves a higher peak gain of 3.88 dBi, 3.87 dBi, and 3.83 dBi and comparatively fewer impedance bandwidths of 14.61%, 5.42%, and 5.40 %, respectively. The antenna resonates at 2.47 GHz, 3.55 GHz, and 5.55 GHz. FR-4 substrate is used to fabricate the antenna. Five Split Ring Resonators (SRRs) units are fabricated on the ground plane, complicating the antenna design. The constructed antenna is suitable for triple-band applications because it combines monopole and SRRs. The total antenna size is $83 \times 56 \times 1.56$ mm^3. A complex metamaterial (MTM) based monopole antenna design is proposed by M. Kasmaei et al. [23], which can function in 3G, WLAN, and WiMAX frequency bands. The antenna covers 2.45 and 5.2 WLAN bands (2.02 - 2.62 GHz and 5.12 - 5.34 GHz) along with 3.5 GHz WiMAX (3.48 - 4.56 GHz) bands. The antenna dimensions are also comparatively larger, $45 \times 40 \times 1$mm^3, built on an FR-4 substrate with a relative permittivity of 4.4. The impedance bandwidths of 600 MHz, 1080 MHz, and 220 MHz and peak gain of 2.23 dB, 2.81 dB and 1.91 dB are obtained at 2.02 - 2.62 GHz, 3.48 - 4.56 GHz, and 5.12 - 5.34 GHz, respectively.

A significant amount of research has been conducted on approaches for increasing bandwidth and gain in hexagonal-shaped patch planar antennas [24-27]. The designs presented by the research community have considerably improved the outcomes by utilising fractal approaches, various feeding strategies such as CPW/coaxial feeding, and SRR (split-ring resonator). However, these techniques make the antenna structure large and bulkier with a complex design. A small 5G reconfigurable antenna for four frequency bands, 2.4 GHz, 3.1 GHz, and 3.4 GHz, presented in [24] provides frequency selectivity through a grouped element switch. The proposed monopole antenna has a small footprint, $37 \times 35 \times 1.6$ mm^3, built on an FR-4 substrate with relative permittivity of 4.3. The proposed configuration can function as an omnidirectional antenna with a bandwidth of 200 MHz, 682 MHZ, 590 MHz and 960 MHz at 2 GHz, 3.4 GHz, 2.45 GHz and 3.1 GHz, respectively. The antenna achieves a peak gain of 1.95 dB only and an efficiency greater

than 85%. A multiband hexagonal patch antenna using an FR-4 substrate consisting of a circular slot on a radiating element and four rectangular slots is proposed in [26]. The antenna resonates at 2.40 GHz, 5.03 GHz, and 8.67 GHz, covering WLAN, WiMAX and X-band. The total antenna dimension is $35 \times 30 \times 1.2$ mm^3 and attains a peak gain of 1.63 dB, 1.38 dB and 2.95 dB in the respective lower, middle and higher bands. A stub-loaded, hexagonal ring patch antenna excited through a triangular shape coplanar waveguide (CPW) transmission line is presented in [27]. The antenna covers WLAN/WiMAX and ITU bands from 2.9 to 5.9 GHz and 7 to 10 GHz. The substrate is made of FR-4 with a thickness of 0.8 mm and a total dimension of 20×20 mm^2. For multiband operation, stubs are attached to the slotted hexagonal patch. But the paper does not discuss the antenna's gain and efficiency parameters.

Although the designs discussed above use the same substrate material, FR-4, they utilise distinct patch and ground geometries and are constructed using different bandwidth enhancement methods. As a result, most antennas are ineffective in one or two operating bands and have comparatively large sizes and moderate gains with complex antenna designs. This article investigates a wide-slot hexagonal shape patch using the DGS plane. A defected ground structure (DGS) reduces antenna size, improves radiation performance, and suppresses cross-polarisation. Slotting is also used, which decreases the antenna volume while increasing the current route length and is also used to maintain the patch's size. The antenna's distinctive feature is its ability to operate across multiple bands using stubs while retaining a compact size and simple structure. The present article evaluates the antenna's performance using frequency domain properties such as gain, reflection coefficient, and radiation patterns. The proposed antenna has adequate efficiency and high gain with compactness while covering wireless LAN, WiMAX, and 5G Sub-6 GHz frequency bands with a simple design that is less bulky, easy to fabricate, and easy to integrate with other devices. Section 2 of the paper discusses the theoretical aspects of the proposed antenna. Antenna working using vector E-field and current distribution has been explained in section 3. An equivalent electric model of the proposed antenna using ADS software is described and compared with the proposed antenna reflection coefficient (S_{11}) in section 4. Simulated and measured results are discussed in section 5, and finally, the paper is concluded in section 6.

2. THEORETICAL ANALYSIS

The proposed monopole antenna structure is straightforward and has a hexagonal shape patch and an equivalent wide hexagonal slot etched through the main patch. Three inverted L-shaped stubs are added to generate the desired resonating frequencies. An inverted L-stub is attached to one of the main hexagon's outer edges, and the other two are within the slotted patch's vicinity. A defected ground plane is etched on the other side of the substrate. There is no ground on the opposite side of the main radiating element, mainly covering the feed line. The following section describes the theoretical dimension calculation for patch, stub and feed lines.

For the wideband antenna, the lower band edge frequency is the fundamental design parameter for monopole antennas rather than the resonance frequency [28]. The lower edge frequency can be determined by comparing the area of the monopole antenna to that of a cylindrical monopole antenna with a comparable height, 'L,' and radius, 'r' [28].

$$f_{LE} = \frac{7.2}{(L_c + P + R_c)\,k}\ \text{GHz} \tag{1}$$

where f_{LE} = lower edge frequency

$\quad R_c$ = radius of the cylindrical monopole antenna in cm

$\quad L_c$ = length of the cylindrical monopole antenna in cm

$\quad P$ = probe length in cm (distance between the partial ground plane and patch vertex)

$\quad k = 1.15$ for the FR-4 substrate having a thickness of 1.6 mm [28].

The patch is fed at its vertex, and the values of above defined L_c and R_c are designed as given below:

$$L_c = 2 * l_h \tag{2}$$

$$R_c = \frac{\sqrt{3 * l_h}}{(8 * pi)} \tag{3}$$

Where l_h is the side length of the hexagon, putting these values in equation (1) and using the value of P and k, the lower edge frequency can be calculated. The first hexagonal patch is constructed with $f_{LE} = 3.6$ GHz to keep the antenna size small. A microstrip transmission line of 50 Ω has been used to feed the hexagon patch. The following equation shows a relation between the microstrip line's size and characteristic impedance Z_c [29].

$$Z_c = \frac{120 * pi}{(\sqrt{\varepsilon_{\text{reff}}})\left\{\frac{W}{H} + 1.393 + 0.667 * ln\left(\frac{W}{H} + 1.444\right)\right\}} \tag{4}$$

Where H is the depth and W is the breadth of the dielectric substrate microstrip feed line. $\varepsilon_{\text{reff}}$ is the effective dielectric constant and is calculated as:

$$\varepsilon_{\text{reff}} = \frac{\varepsilon_r + 1}{2} \tag{5}$$

The current path length has to be extended to generate the fundamental mode in the desired frequencies. Therefore, stubs are used whose length determines the resonating frequency. The lengths of the stubs may be changed to obtain the desired resonance frequency and can be adjusted separately without affecting the main patch characteristics. Three L-subs are attached with the main patch to cover Wi-Fi/WLAN and WiMAX frequency ranges. The stub length is optimised to be close to the quarter wavelength of the resonant frequency for f_l=2.45 GHz and f_h=5.5 GHz, using equation (6-7) [29].

$$L_{1@2.45} = \frac{c}{4 * f_l \sqrt{\varepsilon_{\text{reff}}}} \tag{6}$$

$$L_{2@5.5} = \frac{c}{4 * f_h \sqrt{\varepsilon_{\text{reff}}}} \tag{7}$$

2.1. Antenna Structure

The final patch antenna with a DGS plane on the ground side and a slotted hexagon antenna with inverted L-stubs are shown in Figure 1 from the top, rear, and side views. The epoxy substrate having $\varepsilon_r = 4.4$ (relative permittivity) and $\delta = 0.02$ (loss tangent) with a thickness of 1.6 mm has been used for fabrication. Table 1 demonstrates the optimal geometric dimensions of the presented antenna. The width of the three inverted L-strips is kept fixed.

The fundamental configuration of the proposed antenna started with a hexagon patch, whose dimensions are obtained using equation (1). The patch has been connected to a 50 Ω microstrip feed line at one of its vertexes. Figure 2(a) shows the initial stage designed antenna that resonates at 4.2 and 7.5 GHz frequencies, has a lower cutoff frequency at 3.66 GHz and has an overall 5.33 GHz impedance bandwidth. On the opposite side of the substrate, the defective ground plane is etched, covering the maximum of the feed line, and no ground exists below the main radiating patch. A greater bandwidth has been attained because of the defected partial ground plane.
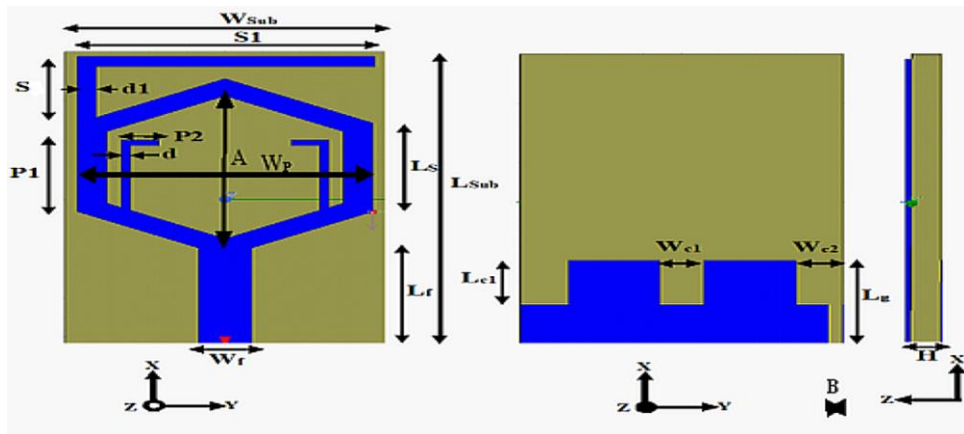
Fig. 1 Final Proposed Antenna
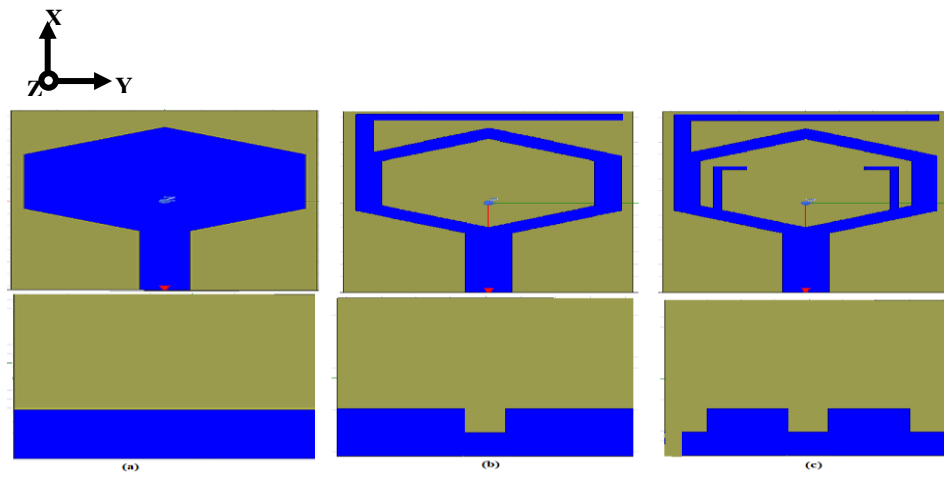
Fig. 2 a) Stage 1; b) Stage 2; c) Stage 3 of the antenna

Table 1 Optimised simulated dimensions of the presented antenna

Symbol	Dimension (mm)	Symbol	Dimension (mm)	Symbol	Dimension (mm)
L_{sub}	30	W_{sub}	17	L_g	9
L_f	10	W_f	2.8	d_1	1
L_S	9	W_P	15.6	H	1.6
L_{C1}	4.5	W_{C2}	2.5	d	0.5
P_1	7	P_2	2	W_{C1}	2.3
S	6.86	S_1	14	B	1.5
A	14.5				

Finally, at stage 3, two inverted L-stubs with length $L_2 = P_1 + P_2$ are extruded in the region of the slotted patch to generate a resonance peak in the $f_h = 5.5$ GHz band, as illustrated in figure 2(c). For greater bandwidth at higher frequency bands, final slots are carved on the ground plane's corner side. The HFSS v.19 simulator is used to model the proposed antenna. Reflection coefficient (S_{11}) characteristics for all three stages are shown in Figure 3.
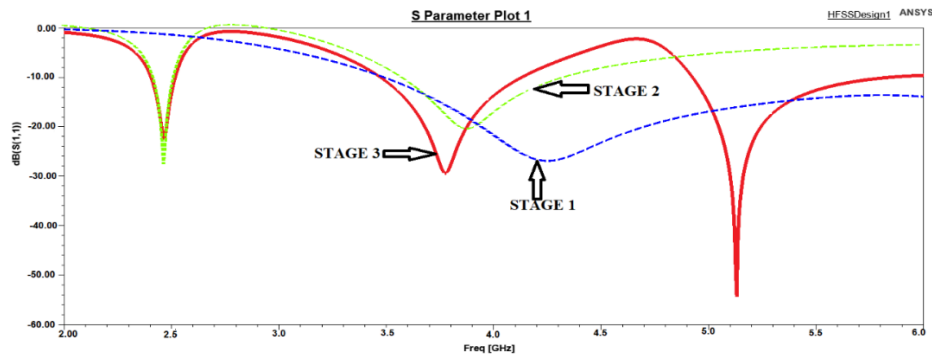
Fig. 3 Reflection Coefficient simulated curves of three phases of the presented antenna

3. ANTENNA OPERATION

Simulated surface current concentration and vector E-field at all three resonating frequencies are depicted in figures 4 and 5, which makes the antenna's working easily understood. The feed line, patch edges, and ground plane edges have the maximum current density. The neighbouring modes must be overlapped with one another to create a broad frequency spectrum. It can be seen from the surface current concentration on the top inverted L-shaped strip at 2.45 GHz and in the middle-inverted L-shaped strip at 5.5 GHz is maximum. From the vector-E plot, it can be concluded that the antenna is linearly polarised and has maximum radiation in the desired direction at desired resonating frequencies. Thus, from the reflection coefficient characteristic (S_{11}) curves and surface current distributions, the purpose of each extended L-strip of the presented antenna can be understood.
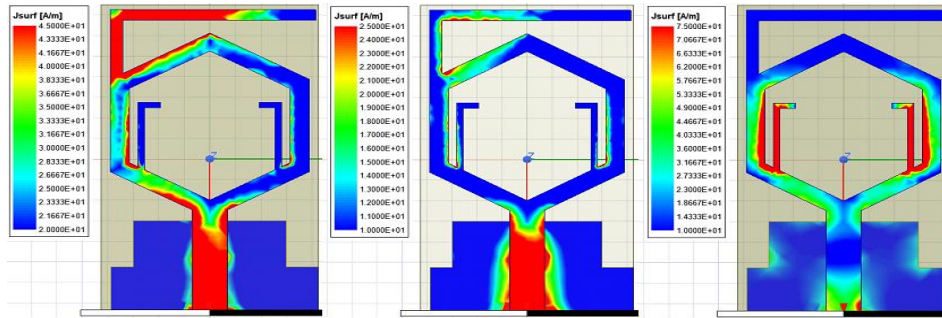
Fig. 4 Simulated current distribution (i) at 2.45 GHz, (ii) at 3.65GHz, and (iii) 5.5 GHz
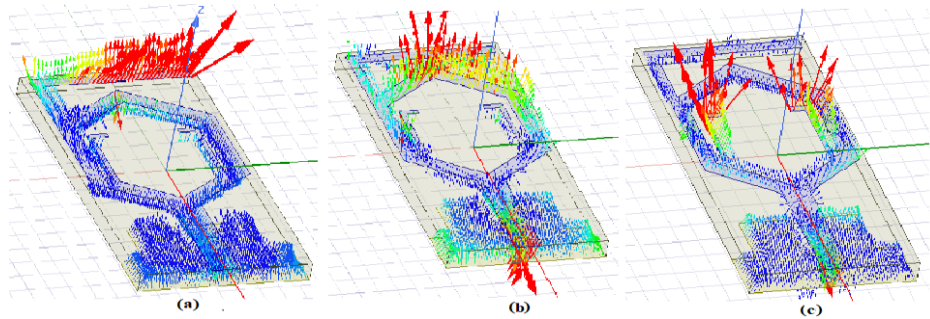
Fig. 5 Simulated E-Vector plot (a) 2.45 GHz, (b) 3.65 GHz, and (c) 5.5 GHz

4. MODELLING OF EQUIVALENT CIRCUIT

The analogous circuit model reveals the characteristics of resonant frequencies and their significance to input impedance. As seen in figure 6, ADS software is used to implement the designed antenna's equivalent circuit model. The antenna reflection coefficient (S_{11}) response is used to create the equivalent circuit model. The reflection coefficient (S_{11}) below 10 dB is optimised to an identical parallel RLC resonant circuit model using Foster's Canonical form. Figure 7 illustrates the contrast between the reflection coefficient (S_{11}) obtained from HFSS and ADS software. The results of the HFSS simulation and ADS are slightly different. The values of capacitors, inductors, and resistors are varied to satisfy the proper response, which causes the shift in resonance frequencies according to the HFSS simulation results.

It can be seen that the results from HFSS and ADS are very well and fairly matched. However, the values at higher frequencies deviate because the equivalent circuit model is roughly compared to 50 Hz. The equivalent circuit-derived values of RLC circuit elements are tabulated in Table 2 for the desired frequency bands. It can be concluded from the above discussion that the surface current distribution, vector E field, and equivalent circuit model provide details of the working of the presented antenna and good insight at resonant frequencies.
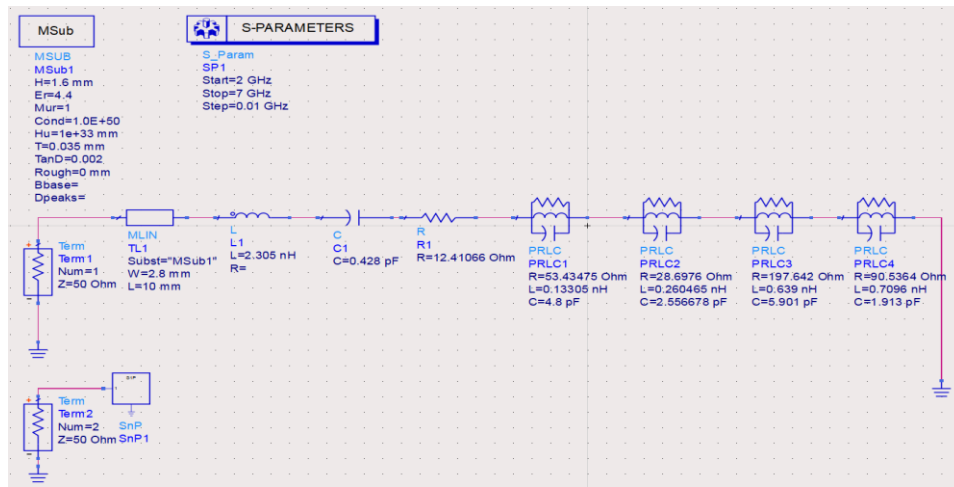
Fig. 6 RLC equivalent circuit modelled in ADS
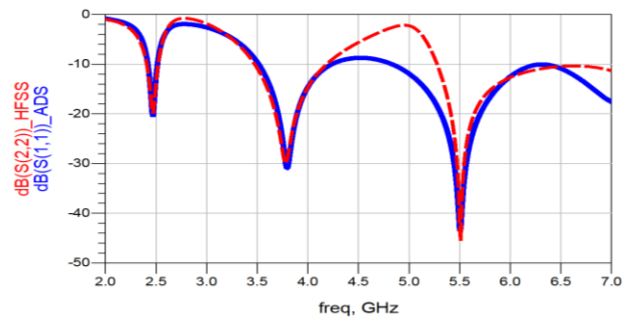
Fig. 7 A comparison of the HFSS and ADS reflection coefficients

Table 2 Equivalent RLC components for the antenna

Parameters	PRLC1	PRLC2	PRLC3	PRLC4
Inductor (nH)	0.133	0.26	0.639	0.703
Capacitor (pF)	4.8	2.55	5.90	1.913
Resistance (ohms)	53.43	28.69	197.6	90.5
L1 (nH)	2.3			
C1 (pF)	0.428			
R1 (ohm)	12.4			

5. PARAMETRIC ANALYSIS

The antenna is subjected to a parametric analysis to determine its ideal dimensions and to improve its performance. This section shows the effects of adjusting the antenna's different geometries. An inverted L-stub length ($L_1=S_1+S$) is attached to the upper side of the radiating element to cover the 2.45 GHz frequency band. The lowest resonating

frequency can be altered by changing the L-stub length without affecting the other resonant frequencies, as shown in figure 8(a). Two inverted L-stubs length ($L_2 = P_1 + P_2$) are appended in the vicinity of the hexagonal slot for resonating the antenna at the 5.5 GHz WLAN band. By changing the length of these L-stubs, the resonating frequency for the 5.5 GHz WLAN band can independently be altered without affecting the lower and mid-frequency bands. Figure 8(b) depicts the change in the resonating frequency by altering the length P_2.

Three slots have been etched on the partial ground plane on the other side of the substrate - the centre slot just below the feed line whose width W_{C1} affects the crust value of the reflection coefficient. Figure 8(c) shows the maximum value of S_{11} is at optimised width, describing a good matching at resonating frequency at all three bands. Figure 8(d) shows the effect on resonating frequencies at middle and higher frequency bands when the width of ground slots at edges varies (W_{C2}). Besides the exception optimised width, the middle and higher resonating frequencies shift toward their higher side with lesser matching as the width increases. The lower frequency band is least affected by the width W_{C2} except for its impedance matching changes.
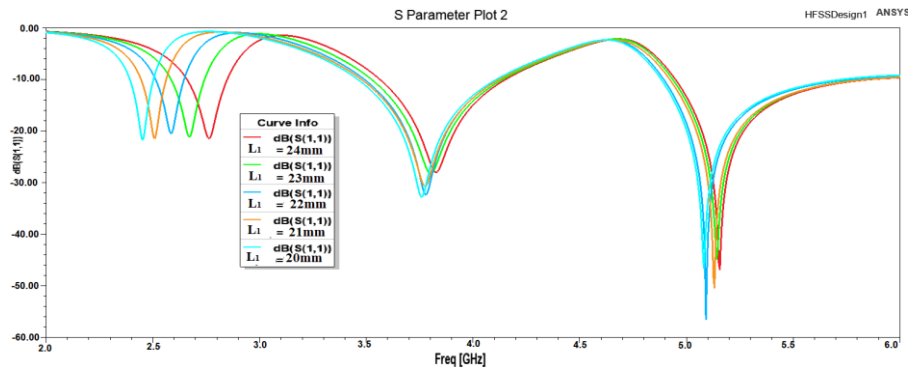
(a) Variation of lower resonating frequency (2.45GHz) w.r.t. L_1
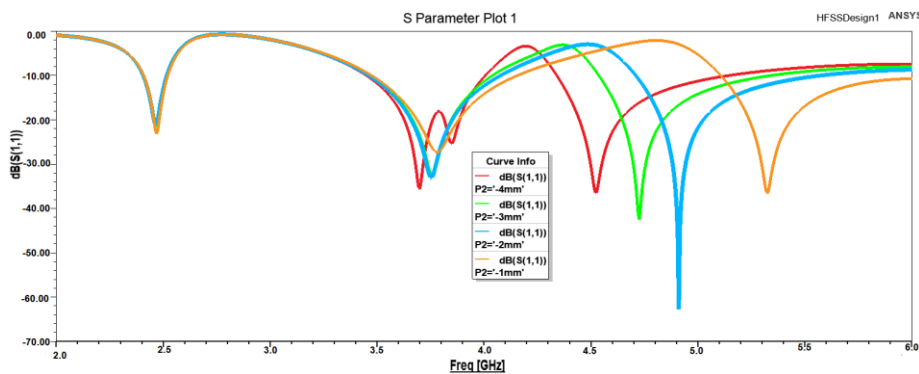
(b) Variation of higher resonating frequency (5.5 GHz) w.r.t P_2
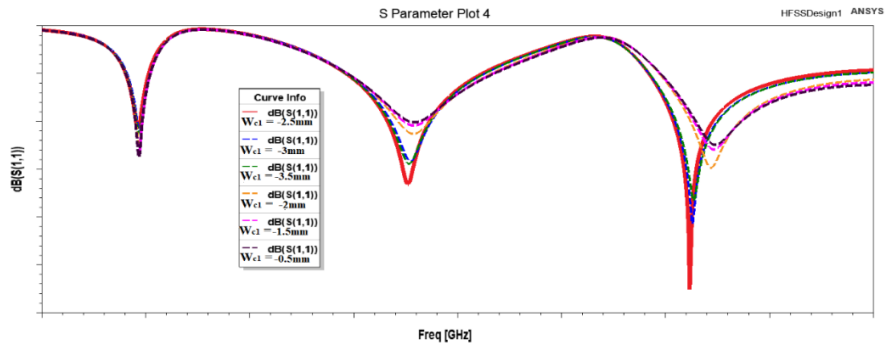
(c) Variation in S_{11} vs. W_{C1}
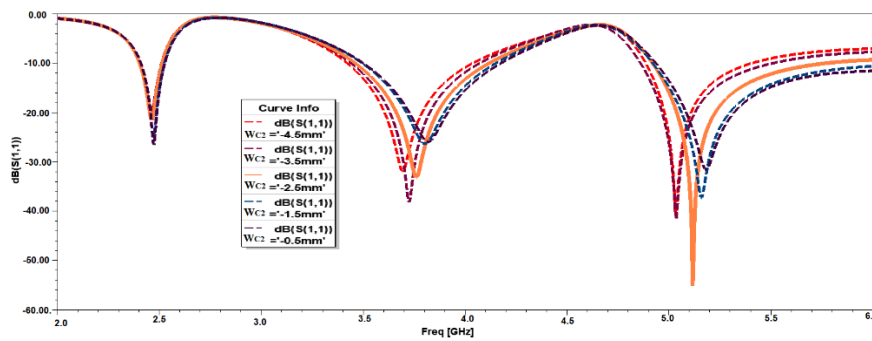
(d) Variation in S_{11} vs W_{C2}

Fig. 8 Parametric analysis by altering. (a) L_1, (b) P_2, (c) W_{C1}, (d) W_{C2}

6. SIMULATED AND MEASURED RESULTS

The focus of this section is the comparison of experimental and simulated outcomes. A prototype antenna is constructed on an FR-4 substrate using the dimensions of Table 1. A female edge-mounted SMA connector with 50 Ω impedance has been used for the excitation of the antenna. The fabricated antenna is tested experimentally, and the findings are compared to the simulated outcomes of the antenna. Figure 9(a-b) shows the fabricated

(a)   (b)
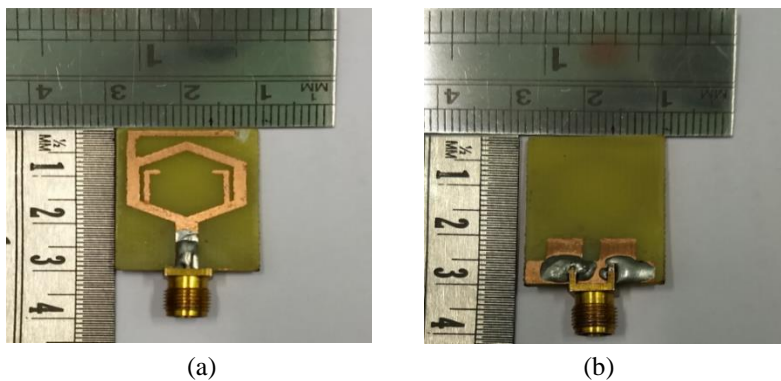
Fig. 9 Fabricated antenna (a) Top Patch, (b) Bottom Ground

antenna's top and bottom surfaces. The antenna characteristics are measured on the VNA KC901C model from Measall Technology. Figure 10 (a) and (b) depict the simulated reflection coefficient (S_{11}) and simulated results against the measured one, and figure 11(a-d) shows the measured reflection coefficient (S_{11}) parameter for all three frequency bands.

(a)

(b)
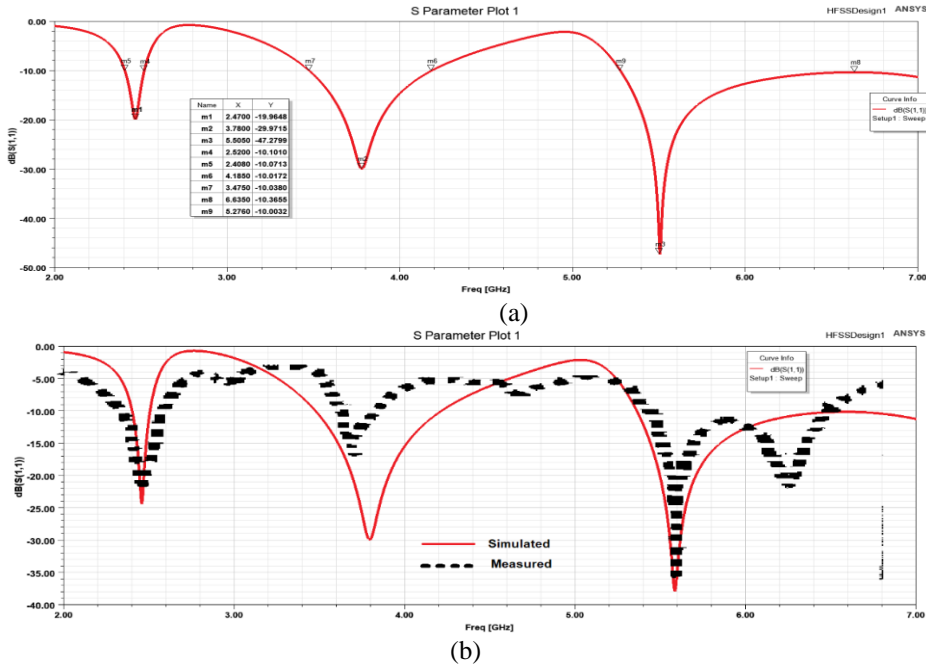
Fig. 10 (a) HFSS generated Reflection Coefficient (S_{11}) (b) Simulated vs Measured S_{11}

The tiny size, fabrication process errors, SMA connection quality, and soldering faults contribute to the simulated and actual results variances. Table 3 compares the resonant frequencies and bandwidths of simulated with measured results.

Table 3 Measured vs Simulated resonant frequencies and bandwidths

	Simulated		Measured	
	Resonant Frequency (GHz)	Bandwidth (MHz)	Resonant Frequency (GHz)	Bandwidth (MHz)
Lower Frequency Band	2.45	112	2.42	280
Mid-Frequency Band	3.78	710	3.7	249
High-Frequency Band	5.5	1359	5.7	1105

Figure 12 (a-e) illustrates the experimental and simulated far-field radiation patterns at the low, mid, and high resonance frequencies in the H-plane ($\varphi=90°$) and the E-plane ($\varphi= 0°$). A bi-directional E-plane and omnidirectional H-plane configuration are observed in all three bands. Due to the increased frequency, the radiation patterns in both planes become distorted and less omnidirectional in H-plane at higher frequencies. Such distortions happen at high frequencies because of the stimulation of higher-order modes. However, the measured radiation patterns are relatively stable in both planes.

(a)

(b)

(c)

(d)
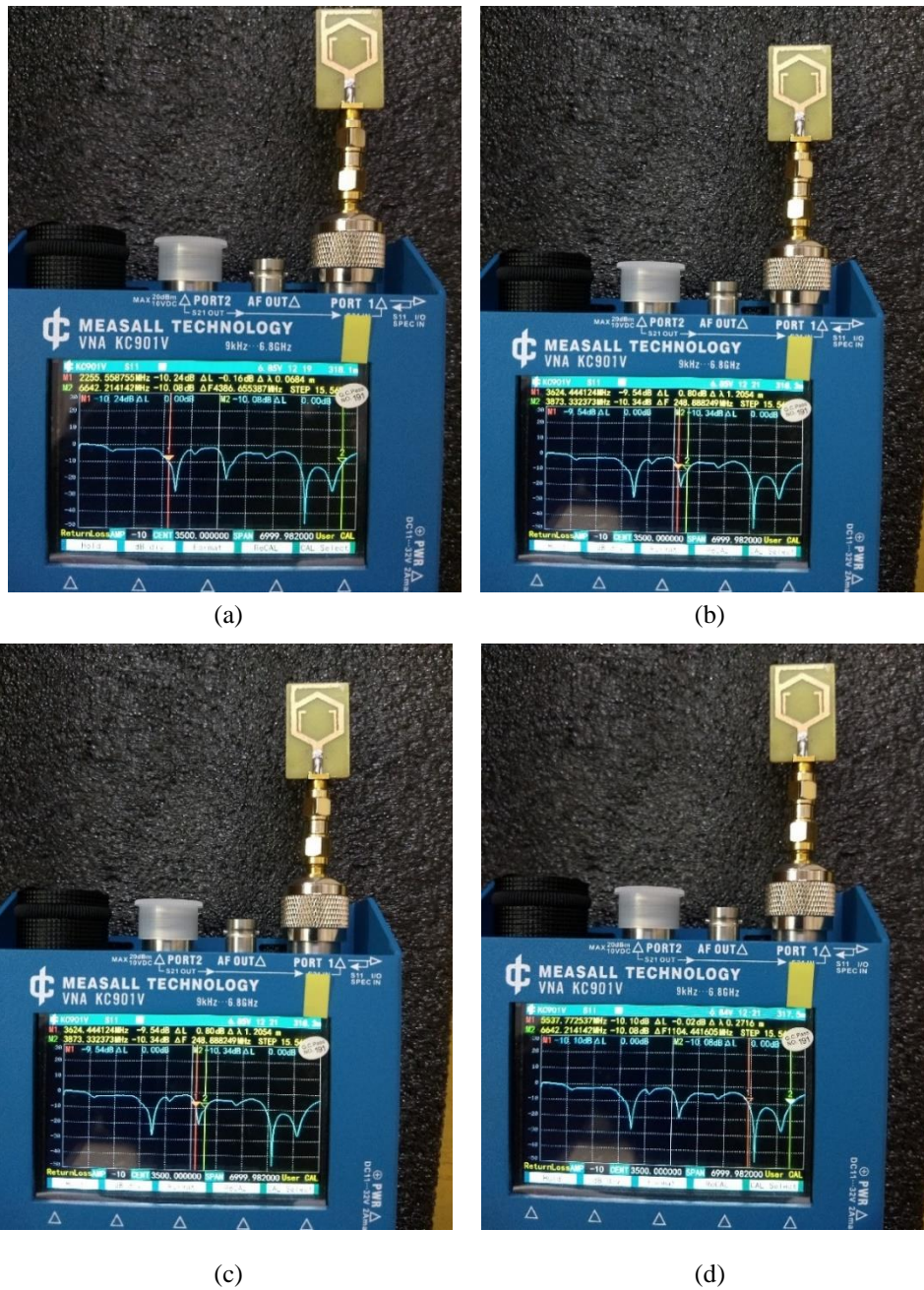
Fig. 11 Measured reflection coefficient (S_{11} in dB) a) Total bandwidth, b) Lower frequency band, c) mid frequency band, d) Higher frequency band
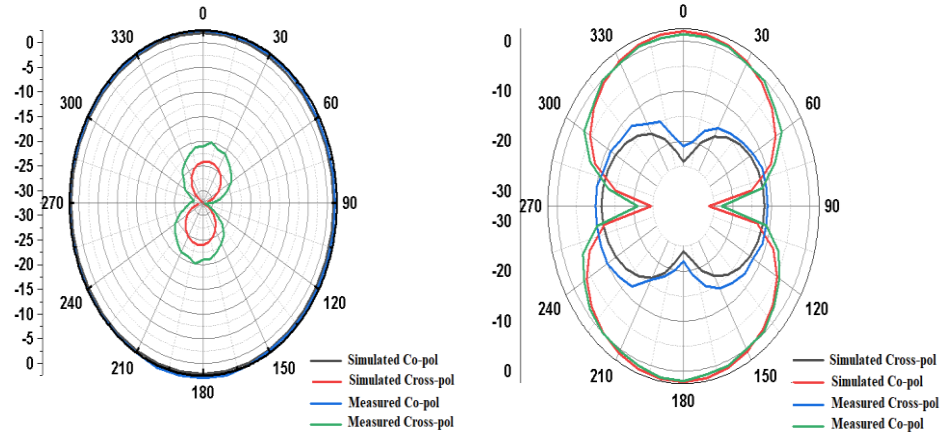
(a) H-Plane (at phi=90°)   at 2.45 GHz   (b) E-Plane (at phi=0°)

(c) H Plane (at phi=90°)   at 3.65 GHz   (d) E Plane(at phi=0°)
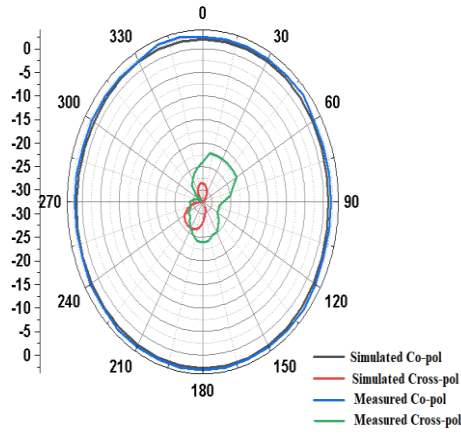
(e) H-plane (at phi=90°)   at 5.5 GHz   (f) E-plane (at phi=0°)
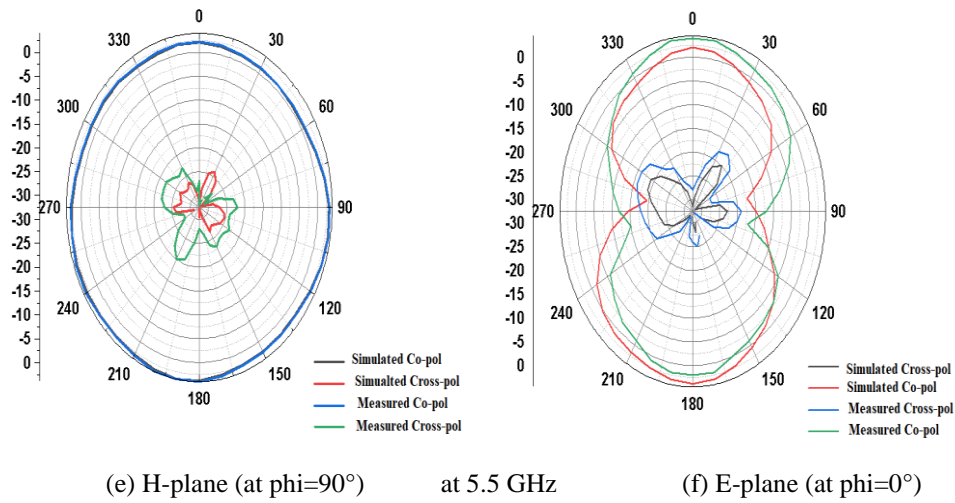
Fig. 12 Simulated and Measured E-plane and H-plane radiation patterns at resonant frequencies

Figure 13 (a) depicts the simulated and measured gain fluctuation. The gain of the proposed antenna is calculated using the gain transfer technique and a standard horn antenna. The measured peak gain is 1.35 dB at 2.45 GHz, 2.55 dB at 3.65 GHz and 3.8 dB at 5.5 GHz. The gain value increases as the frequency increases. Thus, the effective aperture grows in proportion to the wavelength. A peak gain of almost 5.5 dB is achieved at 6 GHz. The simulated gain ranges from 1.5 to 5.8 dB, and the measured gain range from 1.5 to 5.5 dB. Figure 13(b) demonstrates the proposed antenna's radiation efficiency w.r.t each frequencies bands simulated on HFSS. The radiation efficiency increases with frequency, with a maximum efficiency of about 96% found in the mid-frequency region.

(a)   (b)
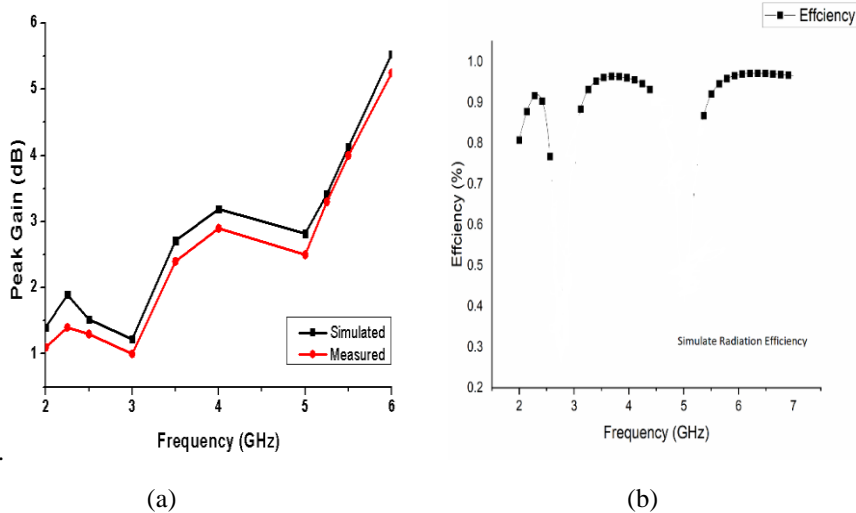
Fig. 13 (a) Simulated and Measured gain in dB, (b) Simulated Efficiency of the presented antenna

The proposed antenna has achieved more than 80% radiation efficiency for all bands. The characteristics of the provided antenna, viz. size, gain, frequency bands, impedance bandwidth, and substrate material, are compared with wideband monopole antenna designs published in recent research articles summarised in Table 4.

Table 4 Comparison of the referenced antenna with the presented antenna

Ref.	Size (mm^3)	Electrical Equivalent Size w.r.t free space wavelength (λ_L)	Operating Frequencies (GHz)	Impedance Bandwidth (MHz)	Peak gain (dB)	Substrate Material
[7]	33×17×1.6	0.55×0.30×0.026	2.5/3.5/5.5	300/400/1520	3.9	FR4
[8]	60×50×1.6	0.72×0.60×0.019	1.8/3.5/5.4	140/180/200	5.18	FR-4
[10]	40×40×1.6	0.64×0.64×0.0256	2.4/3.5/5.5	360/400/450	3.3	FR-4
[11]	36×39×1.6	0.58×0.63×0.026	2.45/3.55/5.5	170/960/740	4	FR-4
[19]	27.5×20×1.5	0.44×0.32×0.024	2.44/3.5/5.5	150/550/2880	4	FR-4
[20]	36×29×0.8	0.59×0.47×0.013	2.45/3.3/5.5	330/140/1060	2.5	FR-4
[21]	34×30×1.6	0.55×0.48×0.026	2.43/3.5/5.7	197/118/90	2.9	FR-4
[22]	83×56×1.56	1.35×0.92×0.0256	2.47/3.55/5.55	380/190/300	3.9	FR-4
[23]	45×40×1	0.64×0.565×0.014	2.12/4.12/5.16	600/1080/220	1.75	FR-4
[24]	37×35×1.6	0.49×0.46×0.021	2/2.45/3.1/3.4	200/590/682/960	1.95	FR-4
[30]	14×16×1.6	0.224×0.256×0.0256	2.4/5.8	400/1500	3.1	FR-4
[31]	12×16×1.5	0.192×0.256×0.024	2.4/5.8	-	1.44	FR-4
This Antenna	30×17×1.6	0.49×0.28×0.026	2.45/3.65/5.5	112/710/1359	5.5	FR-4

7. CONCLUSION

This research article has evaluated and experimentally validated a compact tri-band antenna encompassing WLAN/WiMAX bands at 5G Sub-6 GHz. The total surface dimension of the antenna is 30×17 mm^2 with a simple design using low-profile FR-4 substrate material and having wideband characteristics. The presented antenna could be operated in three bands, resonating at 2.45 GHz, 3.65 GHz, and 5.5 GHz by extruding three inverted L-shaped extensions from the slotted primary patch antenna. Peak gains of 1.34 dB (at 2.45 GHz), 2.55 dB (at 3.65 GHz), and 3.8 dB (at 5.5 GHz) have been achieved. The presented antenna achieved a peak gain of 5.5 dB in the upper-frequency region. The wide bandwidth has been accomplished successfully using defected ground plane while keeping the overall antenna volume minimum. A good impedance matching is obtained by etching an equivalent hexagon slot in the main radiating patch for all the operating bands. The omnidirectional H-plane and bi-directional E-plane with stable gain across the operating frequencies band have also been accomplished. The proposed antenna is a good choice for near-future 5G Sub-6 GHz application systems and WLAN and WiMAX bands because of its compact size, stable gain, and more than 80% efficiency.

REFERENCES

[1] K. F. Lee and K. F. Tong, "Microstrip patch antennas: basic characteristics and some recent advances", In *Proceedings of the IEEE*, vol. 100, no. 7, pp. 2169-2180, 2012.

[2] R. B. Waterhouse, *Microstrip Patch Antennas: A Designer's Guide: A Designer's Guide*, Springer Science & Business Media, 2003, Chapter 4-5, pp. 167-274.

[3] N. Kishore and A. Senapati, "5G smart antenna for IoT application: A review", *Int. J. Commun. Syst.*, vol. 35, no. 13, p. e524, Jan. 2022.

[4] W. Zaman, H. Ahmad and H. Mehmood, "A miniaturised meandered printed monopole antenna for triband applications", *Microw. Opt. Technol. Lett.*, vol. 60, no.5, pp. 1265-1271, 2018.

[5] R. N. Tiwari, P. Singh and B. K. Kanaujia, "Asymmetric U-shaped printed monopole antenna embedded with T-shaped strip for Bluetooth, WLAN/WiMAX applications", *Wirel. Netw.,* vol. 26, no.1, pp. 51-61, 2020.

[6] H. Ahmad, W. Zaman, M. Rehman and F. C. Seman, "The smallest form factor monopole antenna with meandered radiator for WLAN and WiMAX applications", *IETE J. Res.*, vol. 68, no. 4, pp. 3010-3018, 2022.

[7] M. Karthikeyan, R. Sitharthan, T. Ali, S. Pathan, J. Anguera and S. Shanmuga, "Stacked T-shaped strips compact antenna for WLAN and WiMAX applications", *Wirel. Pers. Commun.*, vol. 123, no. 2, pp. 1523-1536, 2022.

[8] A. S. Elkorany, A. N. Mouse, S. Ahmad, D. A. Saleeb, A. Ghaffar, M. Soruri, M. Dalarsson, M. Alibakshikenari and E. Limiti, "Implementation of a Miniaturised Planar Tri-Band Microstrip Patch Antenna for Wireless Sensors in Mobile Applications", *Sensors,* vol. 22, no. 2, p. 667, 2022.

[9] J. Park, J. Minjoo, N. Hussain, S. Rhee, P. Kim and N. Kim, "Design and fabrication of triple-band folded dipole antenna for GPS/DCS/WLAN/WiMAX applications", *Microw. Opt. Technol. Lett.*, vol. 61, no. 5, pp. 1328-1332, 2019.

[10] U. Patel, M. Parekh, A. Desai and T. Upadhyaya, "Wide slot tri-band antenna for wireless local area network/worldwide interoperability for microwave access applications", *Int. J. Commun. Syst.*, vol. 34, no.12, p. e4897, 2021.

[11] S. Wang, F. Kong, K. Li and L. Du, "A planar triple-band monopole antenna loaded with an arc-shaped defected ground plane for WLAN/WiMAX applications", *Int. J. Microw. Wirel. Technol.*, vol. 13, no. 4, pp. 381-389, 2021.

[12] A. Z. Manouare, S. Ibnyaich, D. Seetharamdoo, A. E. Idrissi and A. Ghammaz, "Design, fabrication and measurement of a novel compact triband CPW-fed planar monopole antenna using multi-type slots for wireless communication applications", *J. Circ. Syst. Comput.*, vol. 29, no. 2, p. 2050032, 2020.

[13] B. Kumar, B. K. Shukla, A. Somkuwar and O. P. Meena, "Analysis of hexagonal wide slot antenna with a parasitic element for wireless application", *Prog. Electromagn. Res. C*, vol. 94, pp. 145-159, 2019.

[14] S. Mahapatra and M. N. Mohanty, "An Optimised Feed Hexagonal Antenna with Defective Ground Plane for UWB Body Area Network Application", *Instrum. Mes. Métrolog*, vol. 20, no. 5, pp. 261-267, 2021.

[15] P. P. Singh and S. K. Sharma, "Design and fabrication of a triple band microstrip antenna for WLAN, satellite tv and radar applications", *Prog. Electromagn. Res. C*, vol. 117, pp. 277-289, 2021.

[16] H. V. Pallavi, G. M. M. Naik, A. P. J. Chandra and Paramesha, "Enhancement of Radiation characteristics in a planar Microstrip patch Antenna using Defected Ground Structure", *Turk. J. Comput. Math. Education (TURCOMAT)*, vol. 12, no. 12, pp. 3157-3166, 2021.

[17] M. H. Reddy and D. Sheela, "A Compact Ultra-Wideband Patch Antenna Using Defected Ground Structure", *3C Tecnología. Glosas de innovación aplicadas a la pyme, Edición Especial*, pp. 567-76, 2021.

[18] P. M. Mpele, F. M. Mbango, D. B. O. Konditi and F. Ndagijimana, "A tri-band and miniaturised planar antenna based on countersink and defected ground structure techniques", *Int. J. RF Microw. Comput.-Aided Eng.*, vol. 31, no. 5, p. e22617, 2021.

[19] H. Ahmad, W. Zaman, S. Bashir and M. U. Rahman, "Compact triband slotted printed monopole antenna for WLAN and WiMAX applications", *Int. J. RF Microw. Comput.-Aided Eng.*, vol. 30, no.1, p. e21986, 2020.

[20] Chandan, "Truncated ground plane multiband monopole antenna for WLAN and WiMAX applications", *IETE J. Res.*, vol. 68, no. 4, pp. 2416-2421, 2022.

[21] A. Ibrahim, N. A. Fazil and R. Dewan, "Triple-band antenna with defected ground structure (DGS) for WLAN/WiMAX applications" *J. Phys.: Conf. Ser.*, vol. 1432, no. 1, p. 012071, IOP Publishing, 2020.

[22] A. Pandya, T. Upadhyaya and K. Pandya, "Tri-band defected ground plane based planar monopole antenna for Wi-Fi/WiMAX/WLAN applications", *Prog. Electromagn. Res. C*, vol. 108, pp. 127-136, 2021.

[23] M. Kasmaei, E. Zareian-Jahromi, R. Basiri and V. Mashayekhi, "Miniaturised triple-band monopole antenna loaded with a via-less MTM for 3G, WIMAX, and WLAN applications", *Int. J. Microw. Wirel. Technol.*, vol. 14, no. 5, pp. 601-608, 2022.

[24] S. Ullah, I. Ahmad, Y. Raheem, S. Ullah and T. Ahmad, "Hexagonal shaped CPW feed based frequency reconfigurable antenna for WLAN and sub-6 GHz 5G applications", In the Proceedings of IEEE International Conference on Emerging Trends in Smart Technologies (ICETST), 2020, pp. 1-4.

[25] R. Mark, N. Mishra, K. Madal, P. P. Sarkar and S. Das, "Hexagonal ring fractal antenna with a dumbbell-shaped defected ground structure for multiband wireless applications", *AEU-Int. J. Electron. Commun.*, vol. 94, pp. 42-50, 2018.

[26] A. O. Fadamiro, J. D. Ntawangaheza, O. J. Famoriji, Z. Zhang and F. Lin, "Design of a multiband hexagonal patch antenna for wireless communication systems", *IETE J. Res.*, vol. 68, no. 3, pp. 1675-1682, 2022.

[27] Z. Khan, R. P. Dwivedi and K. U. Kiran, "Stub loaded compact hexagonal ring antenna for WLAN/WiMAX/ITU applications", In the Proceeding of TEQIP III Sponsored IEEE International Conference on Microwave Integrated Circuits, Photonics and Wireless Networks (IMICPW), 2019, pp. 98-102.

[28] G. Kumar and K. P. Ray, *Broadband microstrip antennas,* Artech House, 2003, Chapter 9, pp. 357-378.

[29] C. A. Balanis, *Antenna Theory: Analysis and Design*, Wiley, 2005.

[30] M. V. Yadav and S. Baudha. "Dual-band miniaturised and modified circular patch radiator for Wi-Fi/WLAN Applications" In the Procedding of IEEE Indian Conference on Antennas and Propagation (InCAP), 2019, pp. 1-4.

[31] S. Baudha, M. V. Yadav and N. Joshi. "Miniaturised dual-band arrow shaped planar antenna", *Telecommun. Radio Eng.,* vol. 78, no. 19, pp. 1719-1728, 2019.